

RSC Advances



This is an *Accepted Manuscript*, which has been through the Royal Society of Chemistry peer review process and has been accepted for publication.

Accepted Manuscripts are published online shortly after acceptance, before technical editing, formatting and proof reading. Using this free service, authors can make their results available to the community, in citable form, before we publish the edited article. This *Accepted Manuscript* will be replaced by the edited, formatted and paginated article as soon as this is available.

You can find more information about *Accepted Manuscripts* in the [Information for Authors](#).

Please note that technical editing may introduce minor changes to the text and/or graphics, which may alter content. The journal's standard [Terms & Conditions](#) and the [Ethical guidelines](#) still apply. In no event shall the Royal Society of Chemistry be held responsible for any errors or omissions in this *Accepted Manuscript* or any consequences arising from the use of any information it contains.



From hydrophobic to hydrophilic polyvinylidene fluoride (PVDF) membranes by gaining new insight into material's properties

E. Fontananova^{*a}, M. A. Bahattab^b, S. A. Aljilil^b, M. Alowairdy^b, G. Rinaldi^c, D. Vuono^c, J. B. Nagy^c, E. Drioli^{a,c}, G. Di Profio^a

Received 00th January 20xx,
Accepted 00th January 20xx

DOI: 10.1039/x0xx00000x

www.rsc.org/

This work provides an easy and versatile strategy to manufacture novel polyvinylidene fluoride (PVDF) membranes by solution casting and phase separation technique displaying tailored physicochemical and microstructural features depending on the opportune combination of functionalization by blending chemical additives (multiwalled carbon nanotubes, MWCNTs) and manufacturing procedure. The systematic study of the effect of (i) polymer concentration, (ii) use of pore forming additive (LiCl), and (iii) type and concentration of MWCNTs, on PVDF crystalline composition and membrane microstructure, highlights the strong relationships of these parameters with the wettability, fouling and transport attributes of the formed membranes. The results provide the key to discriminate membrane preparation conditions favoring hydrophilic, low fouling, and highly selective PVDF-MWCNTs membranes, for water-treatment applications in pressure-driven membrane operations, from conditions favoring the formation hydrophobic and waterproof membranes, to be used in the membrane contactors field. Also, they open exciting perspectives for a more effective development of PVDF-based nanostructured membranes for advanced separations based on a comprehensive investigation and understanding of material properties.

Introduction

Modern chemical industry requires advanced separations to boost up production efficiency and product quality according to process intensification strategy.¹ In this context, improved membrane materials, displaying tailored chemical functionalities and engineered structure at multi-scale level, would provide improved separation ability (selectivity), enhanced transmembrane flux and reduced fouling (productivity), compared to traditional ones. Among the different membrane-forming materials, one of the most used is the polyvinylidene fluoride (PVDF) (Figure 1). PVDF is a semicrystalline material with four possible conformations named as α , β , γ , and δ phase.²⁻⁵ The C-F bonds are polar and the highest dipole moment is obtained with the alignment of all dipoles of the polymer in the same direction, corresponding to the β -phase of the PVDF. The dipole moments of α crystallites are oriented in opposite directions, resulting in a zero net polarization. PVDF has outstanding properties in terms of thermal stability, chemical resistance and processability to form membranes by casting solution methods.³⁻⁵ Thank to these features, applications of PVDF

membranes are currently found in pressure-driven water- and waste-treatment treatment (e.g., microfiltration, ultrafiltration and membrane bioreactor), and membrane contactors operations (e.g., membrane distillation, acid gas absorption and stripping, volatile organic compounds removal).³ Despite its attractiveness as high performing polymer material, the performances of PVDF membranes are substantially limited by fouling in the case of pressure-driven membrane operations,^{6,7} and wetting in membrane contactors applications.^{3,8} To mitigate these problems, hydrophilic modification of PVDF has been currently adopted with the aim of reducing fouling, while enhanced hydrophobicity would improve wetting-resistance. These modifications can be achieved during membrane synthesis by blending the polymer with chemical modifiers. Hydrophilic polymer (e.g. polyvinylpyrrolidone) or inorganic particles (e.g. TiO₂, ZrO₂ and carbon nanotubes, (CNTs) can be used to enhance hydrophilicity.⁹⁻¹² More more hydrophobic polymers (e.g. perfluoropolymers) or co-polymers with higher fluorine content than the homopolymer (e.g. polyvinylidene fluoride-co-hexafluoropropylene) can be used to increase membrane hydrophobicity.^{3,13} In alternative, PVDF membranes can be post-treated after manufacture. This can be achieved by hydrophilization through physical surface modification (e.g. coating with a hydrophilic polymer layer) or chemical treatment (e.g. plasma grafting of polar groups).^{4,13-16} Hydrophobicization by coating with a superhydrophobic layer or grafting of fluorinated species is also possible.³ Furthermore, surface roughness modulation is known to

^a Institute on Membrane Technology of the National Research Council of Italy (ITM-CNR), Via P. Bucci, cubo 17/C, University of Calabria, 87036 Rende (CS), Italy. Email: e.fontananova@itm.cnr.it

^b King Abdulaziz City for Science and Technology (KACST), P.O. Box 6086, Riyadh-11442, Saudi Arabia

^c Department of Environmental and Chemical Engineering (DIATIC), University of Calabria, 87036 Rende (CS), Italy

provide additional options to tailor the hydrophobic/hydrophilic character of the membrane surface.^{17,18}

Despite the numerous progresses in the production and modification of PVDF membranes, a comprehensive study on the combined effects of the polymer crystalline phase and surface roughness on hydrophobic/hydrophilic behaviour and transport properties of PVDF membranes, at the best of our knowledge, has not been reported yet. This is particularly important in the case of membranes containing low percentage of functional additive (<3 wt.%). Often the increase of hydrophilicity of composite or mixed matrix membranes prepared by blending inorganic filler with the polymer is attributed to the presence of polar groups on these additives. It is interesting to note that graphitic carbon nanomaterials like CNTs and graphene oxide (GO) are usually introduced at lower content (≤ 2 wt.%) in composite membrane in comparison to three-dimensional inorganic nanofillers like TiO₂ and ZrO₂ (usually blended at loading ≥ 5 wt.%, up to 60 wt.%) , because of their high specific surface, elevated aspect ratio, and the intrinsic properties of graphitized structure.¹⁹⁻²² In addition, the relatively easy functionalization of the surface of carbon nanomaterials render them ideal candidate to tailor the polymer/nanofiller interface in mixed matrix membranes. Zhang¹¹ prepared PVDF mixed matrix membranes containing 1wt.% of CNTs and/or GO observing a relevant decrease of the water contact angle and an increase of water flux in comparison with the polymeric membranes. These results are attributed mainly to the presence of oxygen containing functional groups on the nanofillers used. Also Silva²³ attributed the changes in surface wettability of PVDF membranes containing CNTs to the chemical composition of the additives used at loading ≤ 1 wt.%.

However, it is necessary to consider that the chemical nature of a component present in large defect with respect to the polymer, it could not be sufficient to explain large changes in membrane properties. On the contrary it is well accepted that a functional additive can influence, also if present at low loading, the properties of the main component of the membranes, i.e. the polymer, during the fabrication process in terms of microstructure, as well as, crystalline content in the case of crystalline or semicrystalline polymers.⁵

In addition to the presence of functional additives in the casting solution, also the membrane preparation conditions (e.g. type of solvent and concentration of the polymer) can influence physicochemical and morphological characteristic of the PVDF membranes, including the polymorphism.²⁴⁻²⁷ However, in the literature works is not reported a clear correlation between the dominating crystalline phases and the performance in separation processes like fouling tendency of the membranes.

Therefore, it is an important challenge to achieve a more comprehensive understanding of the relationship between the physicochemical and morphological properties of PVDF membranes with their performance.

In this work we propose two different strategies (namely, protocol A and B) to manufacture PVDF-based membranes

displaying tailored physicochemical and morphological properties, by selecting the optimum combination between functionalization by blending chemical additives (multiwalled carbon nanotubes (MWCNTs)) and membrane preparation conditions. A systematic study on the effect of: (i) polymer concentration, (ii) use of pore forming additive (LiCl), and (iii) type and concentration of MWCNTs, is performed with the aim to develop PVDF membranes with tuneable properties selected for specific applications, such as water- and waste-treatment by pressure-driven operations (hydrophilic, low fouling, highly selective membranes) or membrane contactors applications (hydrophobic, waterproof membranes).

The results open exciting perspectives for further progress in PVDF membranes design and development for advanced separations based on a deep understanding and a fine modulation of material properties.

Experimental

Membranes preparation

Polyvinylidene fluoride homopolymer Solef 6010 from Solvay Solexis (melting point 170-175°C, Mw 300-320 KDa, M_w/M_n 2.1-2.6)²⁸ is used as membrane material. N,N-dimethylformamide (DMF, Sigma-Aldrich) is used as solvent and distilled water as non-solvent in the coagulation bath.

The membranes are prepared by non-solvent induced phase separation (NIPS). Two different protocols are developed to prepare porous membranes: in the protocol A, the polymer concentration is 15 wt. %; in the protocol B the polymer concentration is 13 wt. %. Moreover, in the protocol B 2 wt. % of LiCl (Sigma-Aldrich) is added in the casting solution as pore forming (Table 1).

The polymeric membranes are prepared dissolving the polymer in DMF under magnetic stirring at 50 °C. Mixed matrix or composite membranes are prepared using MWCNTs with different properties: pristine (i.e. as synthesized), purified, functionalized by oxidation procedure, and thermally treated. Synthesis, purification and oxidative functionalization of the MWCNTs, are described elsewhere²¹. In addition to procedure previously described, the MWCNTs used in this work are treated by ball milling for 12 hours. Thermal treatment of the MWCNTs is carried out on the purified sample into a quartz tube reactor flushed with nitrogen (460 NmL/min) for 4 hour at 900°C.

For the preparation of the composite membranes, the appropriate quantity of MWCNTs is added to the homogeneous polymeric solution and finally sonicated for 2 hours before casting (ultrasonic bath VWR USC-600-TH 45 kHz, 400 W; an ice bath is used to cool the solution against solvent evaporation). Each solution is cast at 350 μ m thickness onto a glass plate by using a manual casting knife (Elcometer 3700), at 20 \pm 2°C. The cast solution is immediately immersed in the water coagulation bath with the instantaneous formation of a solid membrane detaching from the glass support. The formed membrane is kept in the coagulation bath for about 2 hours and then removed and immersed in another bath of distilled water for additional 24 h to remove residual traces of solvent

and LiCl, if present. Finally, it is stored in distilled water until the use. All the membrane samples are prepared and characterized in duplicate to assess the reproducibility of the results. If not specified, the estimated relative error was $\leq 5\%$ for all the data reported.

Dispersion test of the MWCNTs in solvents

The pristine, purified, thermally treated, and functionalized MWCNTs are dispersed at a concentration of 0.2 wt. % in the following solvents: N,N-Dimethylacetamide (DMA), DMF, or N-Methyl-2-pyrrolidone (NMP). The dispersions are sonicated for 1 hour before visual observation at different times.

Membranes characterization

The membranes cross-section and surface morphology are observed by a FEI Quanta 200 Philips SEM instrument. Cross-sections are prepared by fracturing the membrane samples in liquid nitrogen.

TEM pictures are taken on a Philips Tecnai10 instrument using 80kV accelerating voltage. The membrane samples are encapsulated in an epoxy resin to be cut by an ultramicrotome. The cut membranes are placed on two microscopy grids for the TEM observation.

Surface roughness of the up surface is assessed by Nanoscope III atomic force microscope (AFM Digital Instruments, VEECO Metrology Group) working in tapping mode. AFM images $10 \times 10 \mu\text{m}^2$ are taken on the up surface. Roughness analysis is performed by Windows Scanning x Microscope software²⁹, by calculating average roughness (R_a), root-mean-square roughness (R_{ms}), and maximum height (R_{max}).

Advancing and receding contact angles are measured on the up surface of the membranes previously dried at room temperature, by growing/shrinking sessile water drop, using a CAM 200 contact angle meter (KSV Instruments Ltd.) equipped with a microsyringe, automatic dispenser, and software for image acquisition and processing. Advancing contact angle (ACA) is measured with the increase in the volume of the droplet (initial volume $3 \mu\text{L}$) by adding water with a constant dosing rate ($1 \mu\text{L/s}$) up to $8 \mu\text{L}$ while capturing images. During the entire measurement, the needle remains attached to the drop so that the portion of the needle inside the drop is maintained as small as possible to minimize droplet adhesion. Receding contact angle (RCA) is measured by reducing the volume of the drop with the same dosing flow rate used in the ACA measurements. Static contact angles (SCA) are measured by depositing a water droplet ($5 \mu\text{L}$) onto the up surface and measuring the contact angle after equilibration (5 seconds). Contact angles are calculated as the average of five different measurements.

Fourier transform infrared spectroscopy (FT-IR) analyses in attenuated total reflectance (ATR) is performed using a Perkin Elmer Spectrum One (Perkin-Elmer), on the up surface of each membrane.

Raman spectra are recorded using a Jasco NRS-5100 micro Raman Spectrometer. The spectra are acquired in the back-scattering geometry. The 532 nm line of the laser with

attenuated power of 0.3 mW, is focused on the sample by means of a 100X objective.

The mean pore diameters is measured by a capillary flow porometer (PMI, Porous Materials Inc. Ithaca, NY) using as wetting liquid 3MFluorinert™ Electronic Liquid FC-40.

The total porosity of the membrane is measured by the gravimetric method at 25°C, determining the weight of water contained in the porous part of the membrane. The porosity (ϵ) is calculated by the following equation:

$$\epsilon = \frac{(w_2 - w_1) / D_w}{((w_2 - w_1) / D_w) + (w_1 / D_p)}$$

where w_1 is the weight of the dry sample, w_2 the weight of the wet sample, D_w the water density (0.997 g/cm^3) and D_p is the polymer density (1.78 g/cm^3)²⁸ for polymeric membrane, or polymer/MWCNTs density estimated considering the fraction of each component and their density assuming the density of the MWCNTs equal to 2.1 g/cm^3 .³⁰

Evaluation of the transport properties and fouling tendency of the membranes

Pure water permeation test are carried out using a dead-end stirred cell having an active filtration area of 14.6 cm^2 , pressurized by nitrogen and operating at room temperature ($25 \pm 3 \text{ }^\circ\text{C}$). After about one hour of stabilization under constant transmembrane pressure (TMP), permeate samples were collected at regular time intervals in order to determine the flux (J) as reported in the following equations:

$$J = \frac{V_p}{t \cdot A}$$

where V_p (L) is the permeate volume; t (h) is the permeation time and A (m^2) is the filtration area.

Blue Dextran (MW 2000 KDa, Sigma-Aldrich) is used for retention test at a concentration of 0.1 g/L in water; the TMP applied during the rejection tests is 1 bar. The rejection ($R(\%)$) is calculated using the following equation:

$$R(\%) = \left(1 - \frac{C_p}{C_r} \right) \times 100$$

where C_p and C_r represent permeate and retentate concentrations, respectively. In each rejection test, 100 mL of feed solution is used and 50 mL of permeate are collected under constant TMP. The feed is continuously stirred by means of a Teflon coated magnetic stir bar to reduce concentration polarization phenomena. The solute concentration in the feed, retentate and permeate is analysed by UV spectrometer (Lambda 650S UV-Vis spectrometer, PerkinElmer). The wavelength of maximum absorption for solute is 610 nm. After retention experiment, the membrane is characterized again by

pure water permeation to calculate the relative flux (J_R) defined as follow:

$$J_R = \frac{J_2}{J_1}$$

Where J_1 and J_2 are respectively the pure solvent flux before and after rejection test. The relative flux can be used to have an indication about the membrane fouling: more J_R is close to 1, less the membrane is fouled.

Results and discussion

One of the main issues in the blending of nanoparticles (including CNTs) during composite membranes synthesis by solution casting methods³¹ is their poor dispersion in most of the solvents used for polymer solubilisation and, as a consequence, in the formed membranes.³² Therefore, the dispersion characteristics of the four different MWCNTs used in this work (pristine, purified, oxidized and thermally treated MWCNTs) are preliminarily tested in polar aprotic solvents in which the PVDF is soluble. The dispersions in DMA, DMF and NMP are visually inspected immediately after sonication and after leaving them in the quiescent state for one day. No appreciable variations of the dispersion degree are observed over this time. Uniform dispersion are obtained with all the three solvent in the case of the purified and oxidized MWCNTs (Figure 2c and d). The presence of polar groups on the oxidized MWCNTs (-OH, -COOH and C=O)²¹ reduces their tendency to aggregate through van der Waals interaction, while forming hydrogen bonds with the solvent, resulting in more homogeneous and stable dispersions. Also the purified sample contains some hydrophilic groups because of the presence of defects and vacancies in the graphitic structure susceptible to nucleophilic attack when in contact with the acid aqueous solution used for the purification step.^{21,33} On the contrary the thermally treated and pristine MWCNTs are dispersed in sufficient way only in DMF (Figure 2a and b). Moreover, the thermally treated MWCNTs are poorly dispersed than the pristine in DMA. The high temperature treatment eliminates most of the organic groups present as defects on the MWCNTs, resulting in a more inert material poorly dispersible in organic solvent and with a high tendency to aggregate. Among the three used solvents, the best performing in terms of MWCNTs dispersion is the DMF while the worst is NMP. In the case of the oxidized MWCNTs stable dispersion in DMF are observed after 3 months (Figure 2f). On the contrary after three months a clear sedimentation of the MWCNTs is observed in the case of the purified MWCNTs (Figure 2e). These observations well agree with the higher capacity of DMF to form hydrogen bonds³⁴ (Table 2), and suggest close solubility parameters between MWCNTs and DMF, in agreement to literature data.³⁵ Accordingly, DMF is selected as solvent for the preparation of the membranes. The four types of MWCNTs are used to prepare composite membranes following protocol A and fixing the carbon nanotubes loading at 1 wt. % (casting solution composition corresponding to A-M-1 in Table 1). In agreement with the preliminary dispersion tests in organic solvent, membranes containing thermally treated MWCNTs show the poorest dispersion in the polymeric matrix (Figure 3a), while the most homogeneous dispersion is obtained with the oxidized sample (Figure 3d). An uniform

black colour is observed in the case of the composite membranes containing oxidised MWCNTs, despite the low amount of additive in the casting solution. Pristine and purified MWCNTs display intermediate dispersion of the MWCNTs (Figure 3b and c). For this reason, the oxidized MWCNTs are selected for further investigation. Composite membranes are prepared following both protocols, A and B, adding different amount of the oxidised MWCNTs: 0.5, 1 and 2 wt. %, in the formed membranes. The resulting membranes show an asymmetric structure with a denser skin layer and a porous structure underneath with finger-like macrovoids developing from the up surface towards the internal layers (SEM images in Figures 4-5).

In the NIPS technique, when the cast liquid film is immersed in the coagulation bath, the homogeneous polymeric solution is initially demixed into two liquid phases because of the diffusive exchanges of the solvent and non-solvent.^{31,36,37} The phase with the higher polymer concentration forms the solid membrane while the phase with the lower polymer concentration gives the porous structure. The exchange of solvent and non-solvent during the demixing stage increases the concentration in the polymer rich phase surrounding the polymer lean phase. The polymer molecules may rearrange their structure until the solidification takes place. However, the rate of the precipitation slows down as the precipitation front moves from the interface with the coagulation bath (where the precipitant reaches earlier a threshold concentration for phase separation) towards the internal layers, resulting in an asymmetric structure.^{31,36,37} A net transport of the polymer perpendicularly to the surface is the result of the high gradient in chemical potential at the interface, resulting in a denser skin layer which hinders the precipitant inlet and solvent outlet to/from the bulk of the membrane.^{31,36,37} The final membrane morphology and microstructure is therefore strongly dependent from the local rate of the solvent/non-solvent diffusion that, in turns, is related to the chemical and physical properties of the systems involved and operative conditions (e.g. activity, viscosity and temperature). In the case of the semicrystalline PVDF, two different mechanisms govern the phase separation process: liquid-liquid demixing and solid-liquid demixing.^{38,39} The membranes prepared by protocol A are characterized by a more compact structure (less porous) with less elongated finger-like macrovoids than those prepared by protocol B (Figure 4-5). Moreover, they present spherical PVDF crystallites formed by the liquid-solid demixing process (polymer crystallization) which precedes the liquid-liquid demixing. On the contrary, a cellular structure is observed in the case of protocol B because of the liquid-liquid demixing occurring at an earlier stage, due to the lower concentration of polymer (13 vs. 15 wt. % in protocol B and A, respectively). Moreover, in the protocol B LiCl is used as pore forming additive.⁴⁰ Because of its solubility both in the solvent (DMF) and in the coagulant (water), LiCl diffuses in the water bath and promotes the non-solvent influx, thus facilitating macropores formation. In addition, LiCl increases the rate of phase separation acting as non-solvent for the polymer.¹³ Despite all the samples are cast at the same initial height of the liquid film (350 μm), the final thickness of the membranes varied as a function of the composition (Table 3 and SEM images in Figures 4-5). As expected, solutions containing a higher amount of polymer form thicker membranes (protocol

A). Moreover, the addition of the MWCNTs up to 1 wt.% heavily reduces the final thickness because of the slower phase separation process (delayed demixing due to the increased solution viscosity which reduces the solvents diffusion rates), providing more time to eliminate the solvent before polymer solidification (kinetic effect on the phase separation).¹³ However, a further increase of the MWCNTs content (up to 2 wt.%) results in thicker membranes because of the increased miscibility gap induced by the MWCNTs, which work as non-solvent for the polymer (thermodynamic effect on the phase separation, i.e. less water is required to induce phase separation).¹³ In the presence of MWCNTs up to 1 wt. %, macrovoids are more extended than in the case of the polymeric samples; this means that they have more time to coalesce before polymer solidification (Figures 4-5). On the contrary, less developed macrovoids are formed as a result of a shorter coalescence time with 2 wt. % MWCNTs. For what concerns surface topography, it is possible to appreciate in the bottom surface of the samples prepared by protocol A a spherulitic morphology (Figure 6b). Smoother down surface are observed in the case of membranes prepared by protocol B (Figure 6d), as liquid-liquid demixing dominates over solid-liquid demixing. From SEM images the up surfaces appear dense and substantially similar for both protocols (Figure 6a and b). On the contrary, AFM analyses highlighted significant effects of the membrane preparation conditions on the roughness of the up surface (AFM images in Figures 4-5 and Table 3). The polymeric membranes prepared by protocol A show higher surface roughness than samples prepared by protocol B. Moreover, the presence of the MWCNTs in the protocol A further increase the surface roughness. An opposite effect is observed in the case of protocol B, i.e., MWCNTs decrease roughness. These differences can be explained considering that the hydrophilic oxygen-containing groups grafted on the MWCNTs tend to migrate toward the interface with the coagulation bath to reduce the interfacial energy during phase separation. The result is an increasing surface roughness because of the rigid cylindrical structure of the MWCNTs. A competitive migration of the LiCl particles toward the surface occurs in the case of the membrane prepared by protocol B, resulting in smoother surface. The MWCNTs diffusivity in the casting solution is expected to decrease with the increasing of the MWCNTs loading because of their more severe aggregation by van der Waals interactions. The membranes prepared by protocol A are characterized by a higher water contact angle, as a consequence of their higher roughness, in agreement with the Cassie–Baxter model which predicts that a hydrophobic surface can be changed to superhydrophobic with an increase in roughness.⁴¹⁻⁴³ As a consequence, composite membranes prepared by protocol A have a relevant potential for application in membrane contactors, where hydrophobic, waterproof surfaces, are required. On the contrary, the membranes prepared by protocol B are less rough and more hydrophilic, resulting as potential candidates for low-fouling applications in liquid phase separations, where fouling can be mitigated by increasing the surface hydrophilicity. Another key aspect to be considered in order to correlate the effect of membrane preparation conditions with the surface wettability, is their influence on the crystalline state of the polymer. The PVDF polymer used in the present work (Solef 6010) is in the α -phase, as revealed by FT-IR spectra showing the typical bands

of this phase (763, 795, 854, 975, and 1384 cm^{-1} ; Figure 7a). However, the crystalline composition of the polymer changes during the membrane fabrication procedure, which includes a solubilisation step at 50°C and successive phase separation. In the case of membranes prepared by protocol A (Figure 7b), FT-IR spectra display the signals of two different phases: α -phase and β -phase (840, 1172 and 1273 cm^{-1}).

Membranes prepared by protocol B (Figure 7c), present only the β -phase peaks and the formation of the most apolar phase of the PVDF, i.e. the α -phase, is prevented because of the presence of LiCl in the casting solutions which favours the formation of the most polar phase by polar interactions with the polymer. These results are in agreement with previous works reporting that solvents with larger dipole moment tended to form polar β phase of PVDF.^{27,44} The higher content of the most polar phase induces a higher wettability of the of the PVDF membranes prepared by protocol B than those prepared by protocol A (contact angles in Table 3). The β -phase content ($F(\beta)$) in the membrane series A is quantified using the following equation^{45,46}:

$$F(\beta) = \frac{A_{\beta}}{(K_{\beta}/K_{\alpha})A_{\alpha} + A_{\beta}}$$

where A_{α} and A_{β} are the absorbance at 763 and 840 cm^{-1} ; K_{α} and K_{β} correspond to the absorption coefficients at the respective wavenumbers, which values are 6.1×10^4 and $7.7 \times 10^4 \text{cm}^2 \text{mol}^{-1}$, respectively. A decreasing intensity of the α -phase bands and an increasing intensity of the β -phase bands, with the increasing loading of MWCNTs is observed (Figure 8). Despite the increase of the polar beta phase going from 0% to 2% of MWCNTs loading in membrane, the contact angle is strongly influenced by the surface roughness and increases with the increasing of the roughness parameters (Table 3).

The preparation protocol has a relevant effect on porous membrane microstructure. Protocol B gives membranes with higher mean pore diameter and total porosity in comparison with protocol A (Table 3). In general, the presence of the MWCNTs in the casting solution reduces the mean pore size of the composites with respect to the polymeric samples. MWCNTs distribution is investigated by a combination of TEM and SEM spectroscopy. TEM images highlight in the dense part of the membrane a fine distribution of the MWCNTs with diameter between 10-30 nm surrounded by the polymer matrix (Figure 9e). The interactions between the MWCNTs and the polymer (hydrogen bonds and electron donor–electron acceptor interactions) reduce the tendency of the carbon nanotubes to agglomerate by π – π attractions. Moreover, it is interesting to note that some MWCNTs form a bridge through the pores. It is possible to speculate that this bridging effect is more relevant in the skin layer, where the pores are smaller, influencing in relevant way the transport through the asymmetric composite membranes. MWCNTs with an apparent larger diameter (30-100 nm) are observed in the macropores of the membrane (Figure 9b-e). The formation of this larger MWCNTs is attributed to the adhesion of a thin polymer layer around the MWCNTs, confirming the good affinity between PVDF and MWCNTs. Several MWCNTs wrapped around the polymer spherulites and/or other MWCNTs are present along the whole membrane cross

section. They are firmly entrapped into the polymer structure as confirmed by the absence leaching out from the membrane during water filtration test, even after long time storage in water (> 1 year). Increasing the loading of the carbon nanotubes in the casting solution it is possible to appreciate an increase of their content in the membrane samples by TEM images (Figure 10). However, membranes prepared with higher loading of MWCNTs (2 wt. %) are characterized by a poor dispersion of the additive with the formation of several aggregates of MWCNTs.

Micro Raman spectroscopy contributed to further characterize the composite membranes. Raman spectra of the oxidized MWCNTs show two characteristic bands at 1345 cm^{-1} and 1579 cm^{-1} , indicated respectively as D-band and G-band^{33,34} (Figure 11a). Moreover, a weak shoulder of the G-band is visible at 1613 cm^{-1} , corresponding to the D' band. The D and D' bands are usually attributed to the presence of amorphous or disordered phase in the carbon nanotubes (e.g. topological perturbations by non-hexagonal rings, functional groups, impurities and vacancies susceptible to nucleophilic attack).^{47,48} The G-band corresponds to the in plane tangential stretching of the carbon-carbon bonds in the graphene sheets. The oxidized MWCNTs are characterized by a lower ratio of the intensity of the G band to the D band, in comparison to the pristine MWCNTs (I_G/I_D are respectively 1.08 vs. 1.22). The oxidative functionalization of the MWCNTs causes etching of the graphitic sheets, resulting in MWCNTs with a large number of defect sites where the oxygen-containing functionalities are present. However, the presence of these groups assures a good dispersion of the MWCNTs in polar solvents. Micro Raman analyses are carried out in several points of the up surface of the composite membranes. In all spectra it is possible to clearly distinguish both the D and G bands of the MWCNTs, but they are found at higher Raman shift values compared to the oxidized MWCNTs, because of the electron donor-acceptor interactions between the fluorine atoms of the polymer and the π -system of the carbon nanotubes. Moreover, micro Raman analyses revealed zones with more intense signals of the MWCNTs in comparison to those of the polymer, and zones where they are less intense (Figure 11b and c, respectively). The former appear at the optical microscope as darker spots distributed on a more clear surface, and correspond probably to membrane pores (with a macrovoid developing just beneath) in which the MWCNTs have a higher local concentration. The clearer zones are related to the dense part of the membrane, composed principally by the polymer. The polymeric and mixed matrix membranes are characterized by pure water permeation test (Table 3) and rejection test using a Blue Dextran (MW 2000 KDa) as model of organic foulant (Figure 12). The composite membranes containing MWCNTs have higher rejection with respect to polymeric membranes, but lower flux. MWCNTs are present both in the porous and solid part of the membrane providing higher selective pathways for solvent transport but increasing also the mass transport resistance. The water transport through the hydrophobic internal channel of a CNTs is known to occur in fast way as a result of the slippage of water on hydrophobic surfaces (strong hydrogen-bonding between water molecules in the nanoconfined environment in which the water molecules tend to recede from nonpolar surfaces).^{49,50} Membranes made of vertically aligned CNTs have been reported to show high permeability enhancement

(> 10 for gases and > 1000 for liquids) than predictions for the transport through the inner channel.^{51,52} However they are usually produced on small scale (from few μm^2 to few mm^2) by long and complex (i.e. expensive) fabrication processes. On the contrary the preparation of membranes containing CNTs by blending techniques, like in this work, are cheaper and easier to be scale-upped. Despite the CNTs are not aligned in the prepared membranes and, as a consequence, only a small portion can be opportunely oriented in order to have transport through the inner core, the CNTs can contribute to the transport of the permeating species, as well as, to the reduction of fouling phenomena, by interactions (attractive or repulsive) of the permeating species with their external graphitic surface. This hypothesis is supported by recent molecular dynamic simulation studies which show a strong curvature dependence of the interfacial friction of water at graphitic interfaces which decreases with carbon nanotube radius increasing for water inside, while increases for water outside, tending to reach the value of water confined between two graphene planes when CNT radii is $\geq 10\text{ nm}$.^{53,54} It is also interesting to note that a similar dependence of the transport properties (analysed in terms of flux and rejection), from the loading of the MWCNTs is observed for both series of samples (Figure 12). The data evidence that the intermediate loading of 1 wt. % allowed to reach better performance. TEM analyses showed that the 1 wt. % loading corresponds to a better distribution of the MWCNTs in the polymeric matrix than 0.5 wt. % and 2 wt. % (Figure 10). The Blue Dextran solution flux of all the PVDF membranes is lower than the pure water flux, because of the higher viscosity. Moreover, concentration polarization and fouling phenomena induced the formation of a boundary layer between the membrane and bulk solution that provides additional resistance to mass transport. Membrane fouling during solution filtration is confirmed by the relative flux values lower than 1 (Table 3). The combined effect of surface roughness and crystalline phase composition on membrane wettability resulted in an increased fouling resistance of the polymeric membrane prepared by protocol B (B-P) in comparison to polymeric membranes prepared by protocol A (A-P). B-P sample is characterized by a lower surface roughness and higher percentage of the β -phase than A-P, and both factors reduce the fouling tendency of the membranes. In the case of the composite membranes prepared by protocol A, the presence of the MWCNTs increased the content of the more hydrophilic β -phase, and this effect dominates the increased surface roughness in term of influence on relative flux that resulted higher than for the polymeric sample. In the case of the composite membranes prepared by protocol B, the presence of the MWCNTs reduced the surface roughness in comparison to B-P increasing the relative flux (only the β -phase is present in all the B-series samples). Finally the inclusion of the MWCNTs in polymeric matrix could contribute to reduce the fouling of both series of composite membranes by the formation of a new interface with the permeating solution in comparison with the polymeric samples, with a certain degree of water slippage at the graphitic surface.

Conclusions

The main goal of this work is to gain more insight into the role of physicochemical and morphological properties of PVDF membranes on the separation performance and fouling control.

Novel porous composite membranes are prepared combining PVDF with oxidised MWCNTs following two different procedures (protocol A or B). The presence of oxygen-containing polar groups on oxidised MWCNTs, results in a good dispersion in the casting solution and, consequently, in the formed porous film, by the establishment of hydrogen bonds with the solvent and the polymer. Experimental results demonstrated that the membrane preparation conditions are heavily influential parameters on the morphology, crystalline phase and transport properties of the porous asymmetric membranes. The membranes prepared by protocol A (higher polymer concentration) are characterized by spherical PVDF crystallites formed by the liquid-solid demixing (i.e. polymer crystallization) which preceded the liquid-liquid demixing. On the contrary, a cellular structure is the result of the liquid-liquid demixing occurring at an earlier stage in the case of the protocol B (lower concentration of polymer and hydrophilic pore forming additive LiCl). The β -form of the PVDF crystallite (the most polar crystalline phase of the PVDF) is the dominant phase in all the membranes produced, but a relevant fraction of α -phase (the most apolar crystalline phase) is formed in the membrane obtained by protocol A. The crystalline composition of the PVDF is influenced by the presence of the LiCl and MWCNTs which favours the formation of the β -phase by polar interactions.

Also, the surface roughness is affected by the membrane formation parameters and MWCNTs loading, resulting in more rough surfaces in the case of the composite systems prepared by protocol A. A relationship between the surface roughness and crystalline composition with the membrane wettability is individuated: increasing surface roughness and the content of α -phase, more hydrophobic membrane are obtained; on the contrary, decreasing surface roughness and increasing the content of β -phase of PVDF, more hydrophilic membrane are formed.

The first type of membranes can be favoured using higher polymer concentration and avoiding the use of polar additives (protocol A).

The second type of membranes can be favoured using more diluted casting solutions and hydrophilic additives (protocol B). All the composite membranes had a lower fouling tendency in comparison with the bare polymeric samples. Moreover, the intermediate loading (1 wt. % of MWCNTs vs. 0.5 or 2 wt.%) resulted in better performance in separation test (higher flux and rejection with lower fouling) because of the better dispersion of these nanostructured additives in the polymer matrix at this concentration.

The membranes produced have remarkable potentialities for possible applications in liquid phase separations (protocol B) or in membrane contactors (protocol A).

Acknowledgements

The work was partially funded by the King Abdulaziz City for Science and Technology (KACST) (project: "CNT-RO and NF membranes for the treatment of aqueous solutions and desalination").

Solvay Solexis (Italy) is gratefully acknowledged for supplying the polymer PVDF Solef 6010.

References

- 1 A. Gorak and A. Stankiewicz, *Annu. Rev. Chem. Biomol. Eng.* 2011, **2**, 431.
- 2 A. Lovinger, in *Poly(vinylidene fluoride) In Developments in Crystalline Polymers-1*, Applied Science Publishers, London, 1982.
- 3 F. Liu, N.A. Hashim, Y. Liu, M.R. Moghareh Abed and K. Li, *J. Membr. Sci.* 2011, **375**, 1.
- 4 G.-D. Kang and Y.-M. Cao, *J. Membr. Sci.* 2014, **463**, 145.
- 5 P. Martins, A.C. Lopes and S. Lanceros-Mendez, *Prog. Polym. Sci.* 2014, **39**, 683.
- 6 M. Tao, F. Liu and L. Xue, *J. Mater. Chem.* 2012, **22**, 9131.
- 7 H. Jang, D.-H. Song, I.-C. Kim and Y.-N. Kwon, *J. Appl. Polym. Sci.* 2015, **132**, 41712.
- 8 A. Mansourizadeh and A.F. Ismail, *Int. J. Greenh. Gas Con.* 2011, **5**, 640.
- 9 J. Zhang, Z. Xu, M. Shan, B. Zhou, Y. Li, B. Li, J. Niu and X. Qian, *J. Membr. Sci.* 2013, **448**, 81.
- 10 J. Ying and B. Deng, *J. Membr. Sci.* 2015, **479**, 256.
- 11 J. Zhang, Z. Xu, W. Mai, C. Min, B. Zhou, M. Shan, Y. Li, C. Yang, Z. Wang and X. Qian, *J. Mater. Chem. A*, 2013, **1**, 3101.
- 12 A. Sotto, J. Kim, J. M. Arsuaga, G. del Rosario, A. Martinez, D. Nam, P. Luise and B. Van der Bruggen, *J. Mater. Chem. A*, 2014, **2**, 7054.
- 13 E. Fontananova, J.C. Jansen, A. Cristiano, E. Curcio and E. Drioli, *Desalination* 2006, **192**, 190.
- 14 E. Fontananova, L. Donato, E. Drioli, L. Lopez, P. Favia and R. d'Agostino, *Chem. Mater.* 2006, **1**, 1561.
- 15 L. C. Lopez, M. G. Buonomenna, E. Fontananova, G. Iacoviello, E. Drioli, R. d'Agostino, P. Favia, *Adv. Funct. Mater.* 2006, **16**, 1417.
- 16 L. Wu, J. Sun and F. Tong, *RSC Adv.* **4**, 2014, 63989.
- 17 J. Sun, L. Wu and F. Hu, *RSC Adv.* **5**, 2015, 40753.
- 18 G. Di Profio, E. Fontananova, E. Curcio and E. Drioli, *Cryst. Growth Des.* 2012, **12**, 3749.
- 19 J. Ying and B. Deng, *J. Membr. Sci.* 2015, **479**, 256.
- 20 Y. Zhu, F. Zhang, Dong Wang, Xian Feng Pei, Wenbin Zhang and Jian Jin, *J. Mater. Chem. A*, 2013, **1**, 5758.
- 21 V. Grosso, D. Vuono, M.A. Bahattab, G. Di Profio, E. Curcio, S.A. Al-Jilil, F. Alsubaie, M. Alife, J.B. Nagy, E. Drioli and E. Fontananova, *Sep. Purif. Technol.* 2014, **132**, 684.
- 22 A. Bottino, G. Capanelli and A. Comite, *Desalination* 2002, **46**, 35.
- 23 T.L.S. Silva, S. Morales-Torres, J. L. Figueiredo and A.M.T. Silva, *Desalination* 2015, **357**, 233.
- 24 J.C.C. Ferreira, T.S. Monteiro, A.C. Lopes, C.M. Costa, M.M. Silva, A.V. Machado and S. Lanceros-Mendez, *J. Non-Cryst. Solids* 2015, **412**, 16.
- 25 P. Martins, A.C. Lopes, S. Lanceros-Mendez, *Prog. Polym. Sci.* 2014, **39**, 683.
- 26 S. Lanceros-Méndez, J.F. Mano, A.M. Costa, V.H. Schmidt, *J. Macromol. Sci. B* 2001, **40**, 517.
- 27 Y. Xiang, L. Xue, J. Shen, H. Lin and F. Liu, *J. Appl. Polym. Sci.* 2014, DOI: 10.1002/APP.41065.
- 28 <http://www.solvayplastics.com>

- 29 I. Horcas, R. Fernandez, J.M. Gomez-Rodriguez, J. Colchero, J. Gomez-Herrero and A.M. Baro, *Rev. Sci. Instrum.* 2007, **78**, 1.
- 30 <http://www.cheaptubes.com/MWNTs.htm>
- 31 Mulder M. In *Basic principles of membrane technology*, Kluwer Academic, 1996.
- 32 M.M. Khan, V. Filiz, G. Bengtson, S. Shishatskiy, M. Rahman and V. Abetz, *Nanoscale Res. Lett.* 2012, **7**, 504.
- 33 P.G. Collins, *Defects and disorder in carbon nanotubes*, in *Oxford Handbook of Nanoscience and Technology: Frontiers and Advances*, Oxford Univ. Press, Oxford, 2009.
- 34 D. W. Van Krevelen, in *Properties of Polymers, Their correlation with chemical structure, Their numerical estimation and prediction from additive group contributions*, Elsevier, Amsterdam, 1990.
- 35 L. Kunsil, H.J. Lim, S.J. Yang, Y.S. Kim and C.R. Park, *RSC Adv.* 2013, **3**, 4814.
- 36 K. Kimmerle, H. Strathmann, *Desalination* 1990, **79**, 283.
- 37 A.K. Hoida and I.F.J. Vankelecom, *J. Appl. Polym. Sci.* 2015, DOI: 10.1002/APP.42130
- 38 D.-J. Lin, C.-L. Lin and S.-Y. Guo, *Macromolecules*, 2012, **45**, 8824.
- 39 M. Sharma, G. Madras and S. Bose, *J. Mater. Chem. A*, 2015, **3**, 5991
- 40 A. Bottino, G. Capanelli and A. Turturro, *Desalination* 1988, **68**, 167.
- 41 R. N. J. Wenzel, *Ind. Eng. Chem.* 1936, **28**, 988.
- 42 A. Cassie and S. Baxter, *Trans. Faraday Soc.* 1944, **40**, 546.
- 43 H.Y.C. Erbil and E. Cansoy, *Langmuir* 2009, **25**, 14135.
- 44 M.-M Tao, F. Liu , B.-R. Ma, L.-X. Xue, *Desalination*, 2013, **316**, 137.
- 45 P. Martins, A.C. Lopes and S. Lanceros-Mendez, *Prog. Polym. Sci.* 2014, **39**, 683.
- 46 R. Gregorio and M. Cestari, *J. Polym. Sci., Part B: Polym. Phys.* 1994, **32**, 859.
- 47 V. Datsyuk, M. Kalyva, K. Papagelis, J. Parthenios, D. Tasis, A. Siokou, I. Kallitsis and C. Galiotis, *Carbon* 2008, **46**, 833.
- 48 M.S. Dresselhaus, G. Dresselhaus, R. Saito and A. Jorio, *Phys Rep.* 2005, **409**, 47.
- 49 G. Hummer, J. C. Rasaiah, J. P. Noworyta, *Nature* 2001, **414**, 188.
- 50 H. Verweij, M.C. Schillo, J. Li, *Small* 2007, **3**, 1996.
- 51 M.S. Mauter, M. Elimelech and C.O. Osuji, *ACS Nano* 2010, **4**, 6651.
- 52 M. Majumder, N. Chopra and J. H. Bruce, *ACS Nano* 2011, **5**, 3867.
- 53 K. Falk, F. Sedlmeier, L. Joly, R. R. Netz and L. Bocquet, *Nano Lett.* 2010, **10**, 4067.
- 54 K. Falk, F. Sedlmeier, L. Joly, R. R. Netz and L. Bocquet, *Langmuir* 2012, **28**, 14261.

Table 1. Composition of the casting solution used to prepare polymeric and composite membranes. Oxidized MWCNTs were used for all the samples, but in the case of the A-M-1, membranes containing also pristine, purified and thermally treated MWCNTs were produced.

Sample code	Casting solution composition				Loading of MWCNTs in the prepared membrane [%]
	PVDF	LiCl	MWCNTs	DMF	
	[wt.%]	[wt.%]	[wt.%]	[wt.%]	
A-P	15	-	-	85	-
A-M-05	15	-	0.08	84.92	0.5
A-M-1	15	-	0.15	84.85	1
A-M-2	15	-	0.31	84.69	2
B-P	13	2	-	85	-
B-M-05	13	2	0.07	84.93	0.5
B-M-1	13	2	0.13	84.87	1
B-M-2	13	2	0.27	84.73	2

Table 2. Hansen's solubility parameters of the solvents used for the dispersion test of the MWCNTs (data from [34]). δ is the total solubility parameter. δ_d , δ_p and δ_h are the contribution of dispersion forces, polar forces and hydrogen bonding to the to the solubility parameter, respectively.

Solvent	Solubility parameters			
	[J ^{1/2} cm ^{-3/2}]			
	δ	δ_d	δ_p	δ_h
DMA	22.1-22.8	16.8	11.5	10.2
DMF	24.9	17.4	13.7	11.3
NMP	22.9	17.9	12.3	7.2

Table 3. Properties of polymeric and composite membranes.

Sample code	Mean pore diameter [μm]	Total porosity [%]	Thickness [μm]	Roughness parameters [nm]			Water contact angles [$^{\circ}$]			Water flux* [$\text{L h}^{-1} \text{m}^{-2}$]	Relative flux [-]						
				R_a	R_{ms}	R_{max}	SCA	ACA	RCA								
				A-P	0.047	72	91	54	68			453	95	101	68	38	0.56
				A-M-0.5	0.026	71	75	87	117			734	115	117	75	1.0	0.89
A-M-1	0.032	71	74	70	86	465	103	108	70	20	0.86						
A-M-2	0.042	72	120	103	130	838	123	125	83	1.8	0.86						
B-P	0.060	78	77	43	57	518	74	79	33	63	0.77						
B-M-05	0.047	82	55	39	54	455	81	84	47	27	0.86						
B-M-1	0.051	82	57	23	29	223	71	77	27	56	0.85						
B-M-2	0.028	81	73	29	37	272	71	71	23	30	0.87						

*Water flux measured at 25°C and TMP 1 bar.

Figures Captions

Figure 1. Structure of the α and β -phase of the PVDF

Figure 2. Images of the dispersion of thermally treated (a), pristine (b), purified (c, e) and oxidised MWCNTs (d, f) in DMA (1), DMF (2) and NMP (3) after 24 hour (a-d) or 90 days (e-f) from the sonication.

Figure 3. Images of the composite membranes prepared by protocol A containing: thermally treated (a), pristine (b), purified (c) and oxidized MWCNTs (d). The loading of MWCNTs in the membrane was 1 wt%.

Figure 4. AFM images of the up surface and SEM micrographs of the cross sections of the polymeric and composite membranes prepared by protocol A.

Figure 5. AFM images of the up surface and SEM micrographs of the cross sections of the polymeric and composite membranes prepared by protocol B.

Figure 6. Up and down surfaces of the composite membranes prepared with 1 wt. % of oxidized MWCNTs by protocol A (a: up and b: down) and by protocol B (c: up and d: down).

Figure 7. FT-IR-ATR spectra of the PVDF polymer (a), polymeric membrane prepared by protocol A (b), and by protocol B (c).

Figure 8. (a) FT-IR-ATR spectra of the polymeric and composite membranes prepared by protocol A (colours legend: green A-P; black A-M-05; violet A-M-1; red A-M-2). The arrows in correspondence of the peaks at 763 cm^{-1} (α -phase) and 840 cm^{-1} (β -phase) indicate the effect of the increasing loading of MWCNTs in the membrane on the peak height. (b) Estimated β -phase content vs. the MWCNTs loading in membrane.

Figure 9. SEM (a-d) and TEM (e) images of the PVDF composite membranes containing 1 wt. % of oxidized MWCNTs (sample code A-M-1). Membrane cross section (a) and particular at higher magnification taken along the section: upper (b), central (c) and bottom part (d). TEM image (e) of the longitudinal section.

Figure 10. TEM images of the longitudinal section of the composite membranes prepared at different loading of MWCNTs by protocol A and protocol B.

Figure 11. Raman spectra carried out on: oxidized MWCNTs (a, black line), dark spot on the composite membrane containing 1wt% of MWCNTs (b, sample code B-M-1, blue line), clear region on the previous sample (c, pink line) and polymeric membrane (d, sample code B-P, red line)

Figure 12. Rejection vs. flux of the polymeric and composite membranes prepared by protocol A (empty symbols) and protocol B (filled symbols). Conditions: Blue dextran solution in water (0.1 g/L); 25°C ; pressure 1 bar.

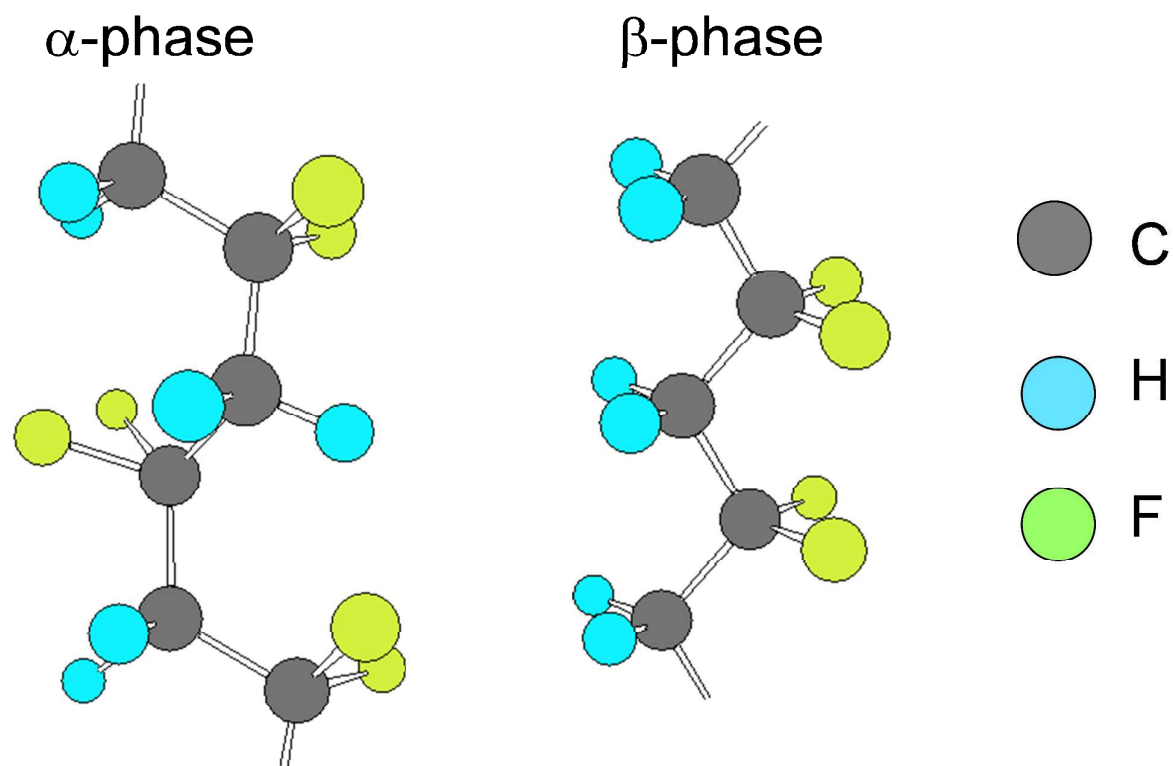


Figure 1

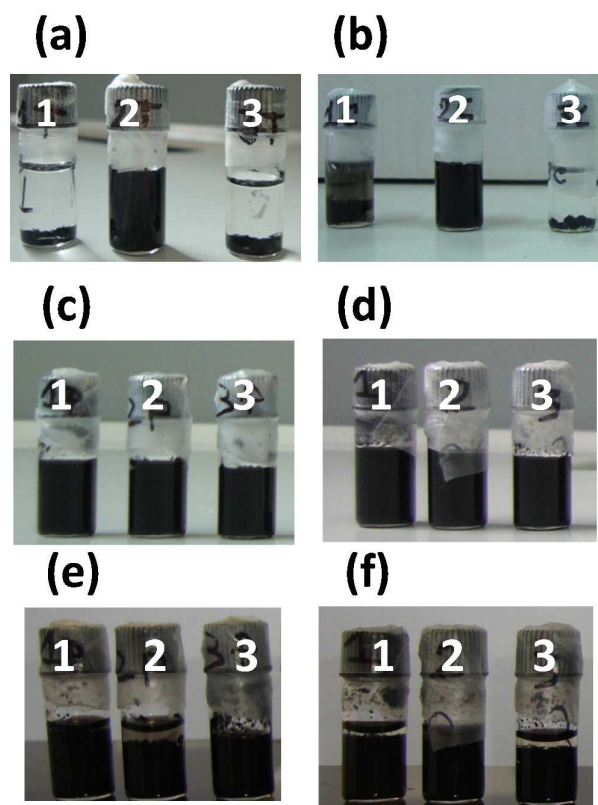


Figure 2

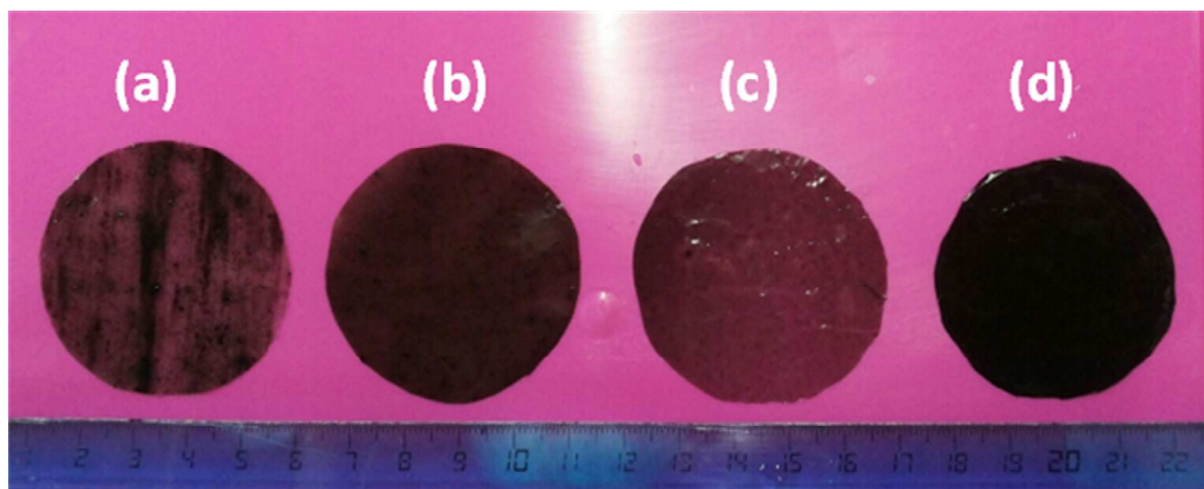


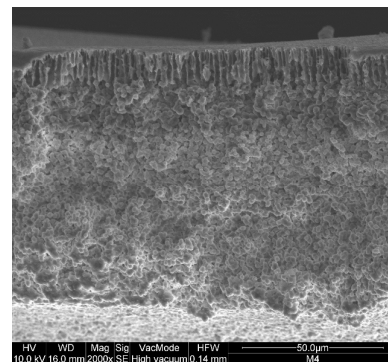
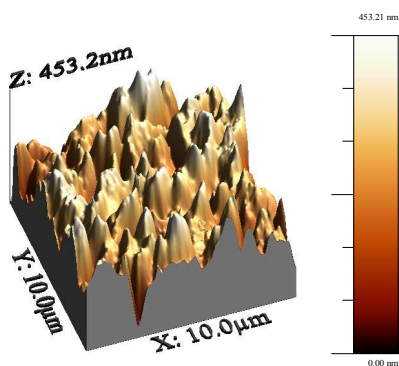
Figure 3

Sample
code

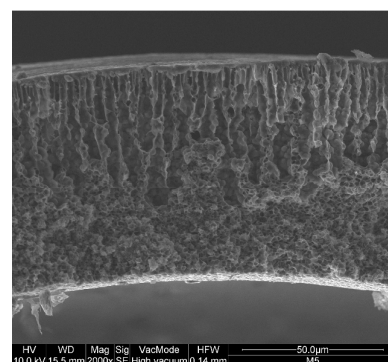
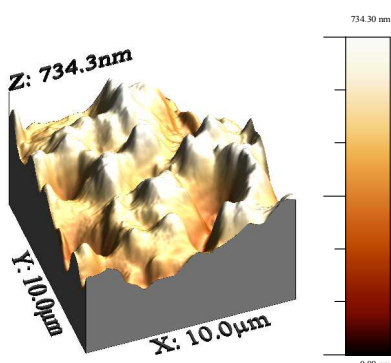
AFM 3D height image of the surface

SEM image of the cross section

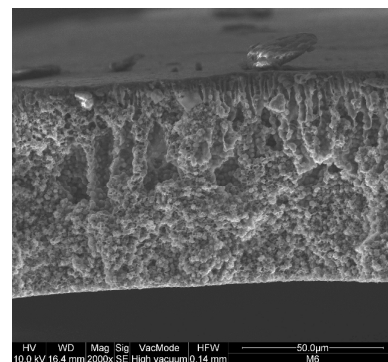
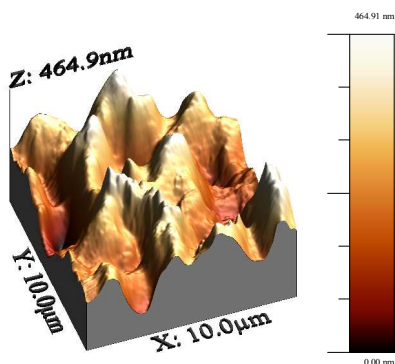
A-P



A-M-0.5



A-M-1



A-M-2

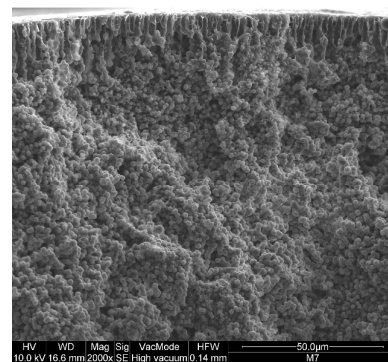
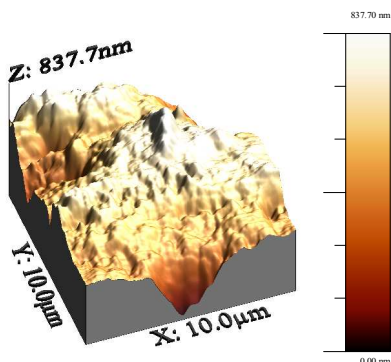


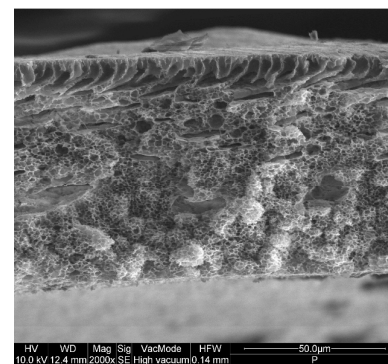
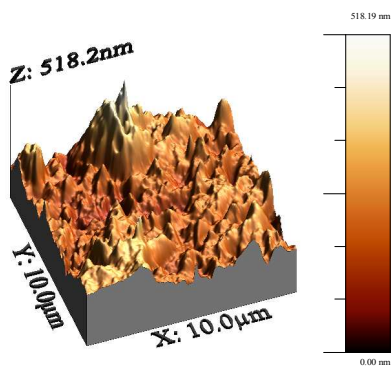
Figure 4

Sample
code

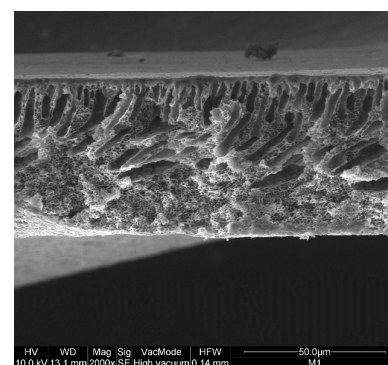
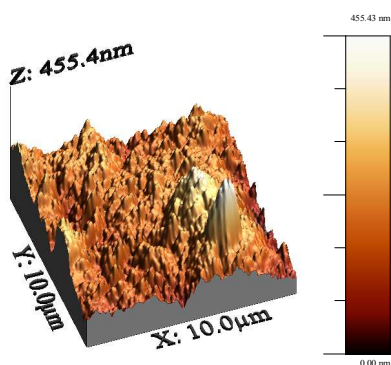
AFM 3D height image of the surface

SEM image of the cross section

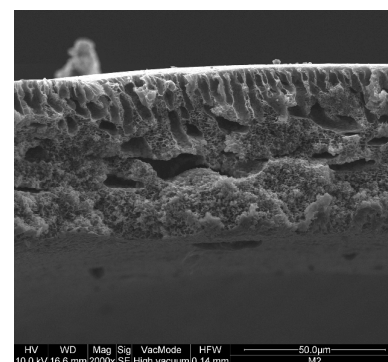
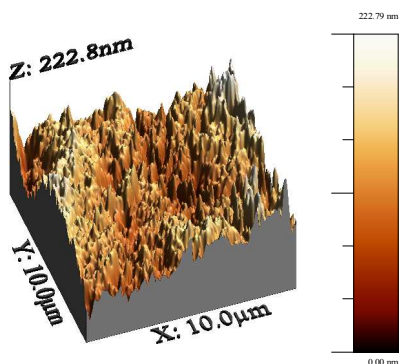
B-P



B-M-05



B-M-1



RSC Advances Accepted Manuscript

B-M-2

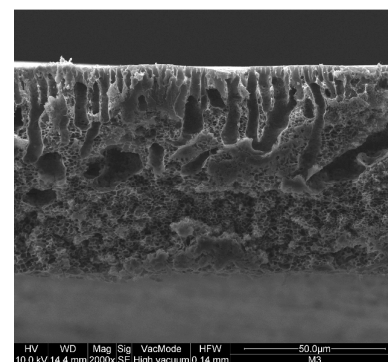
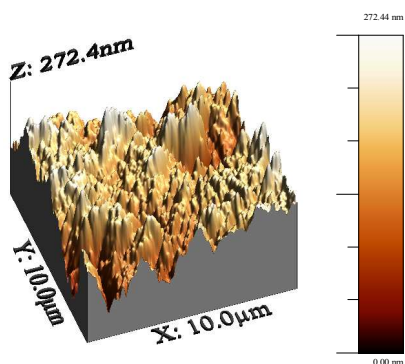


Figure 5

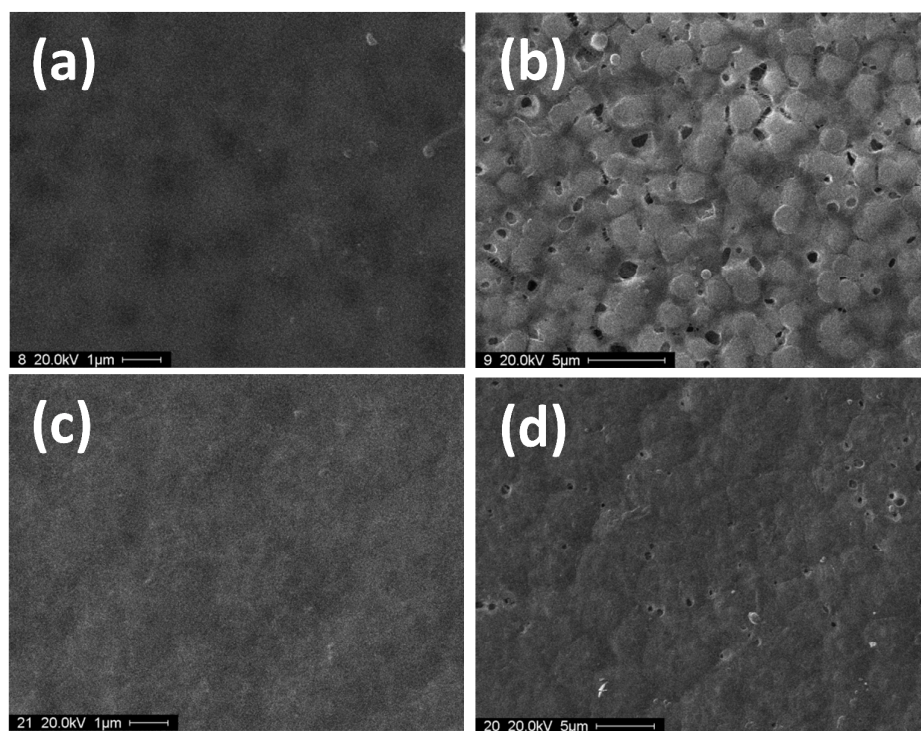


Figure 6

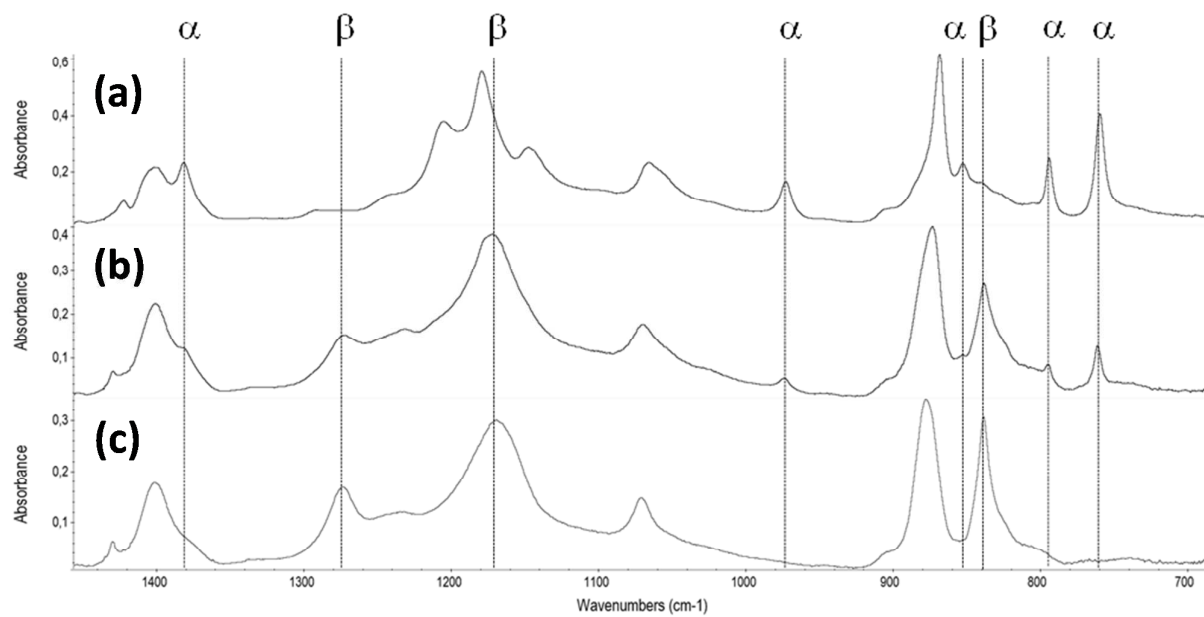
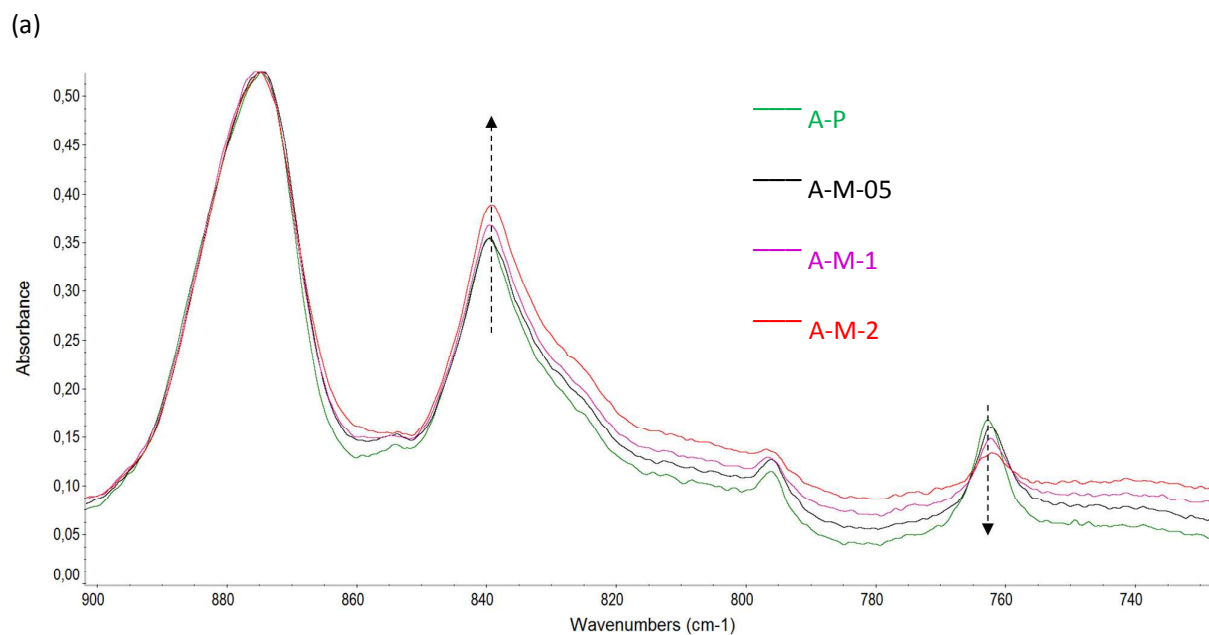


Figure 7



(b)

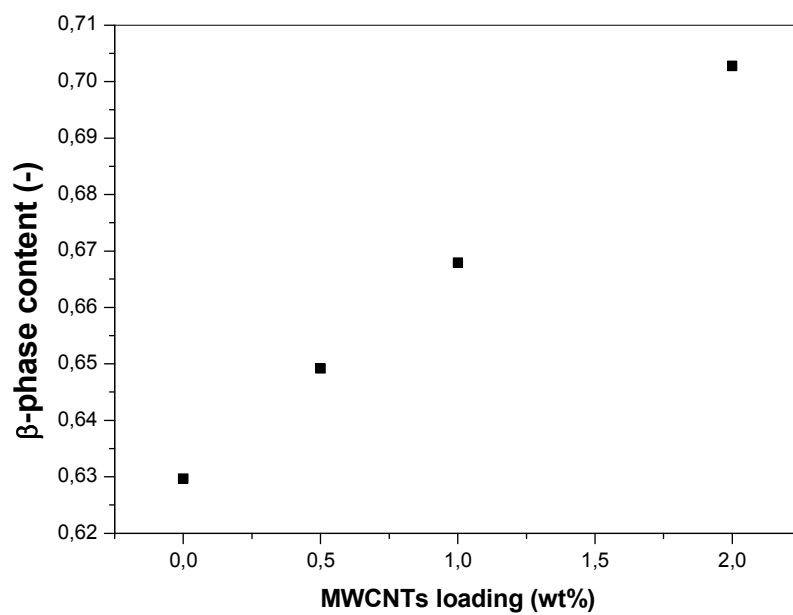


Figure 8

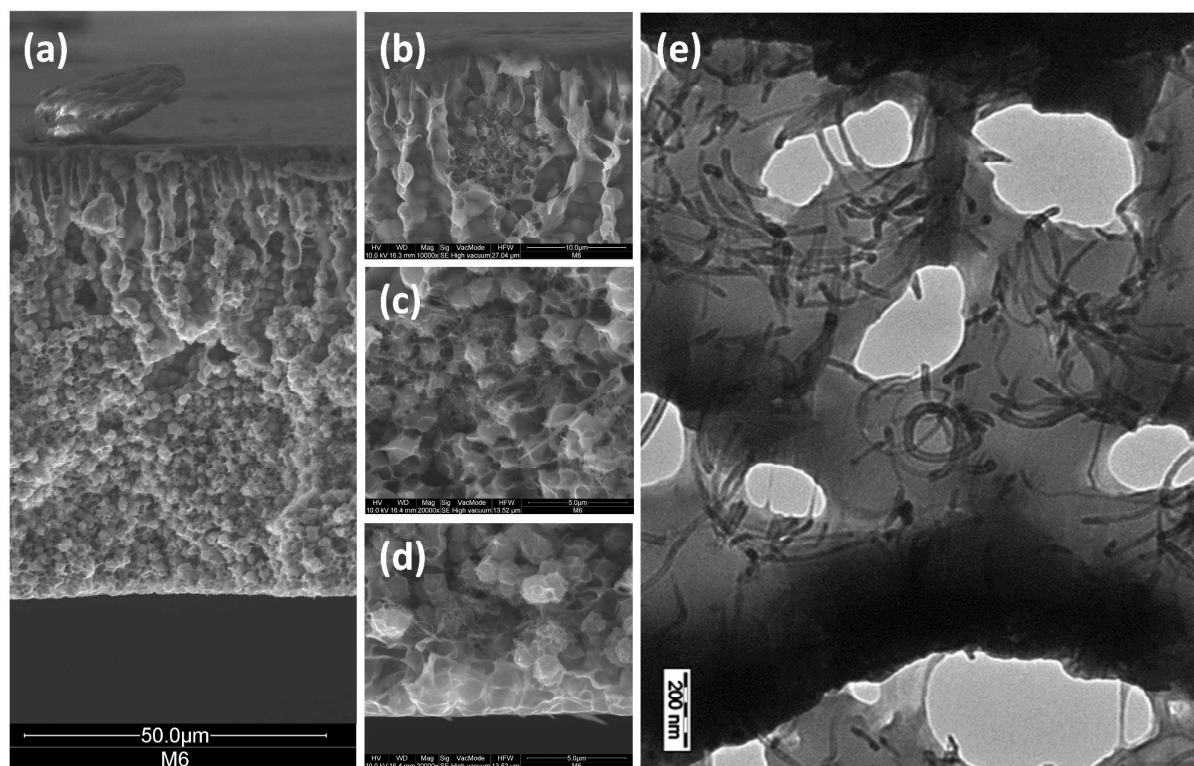


Figure 9

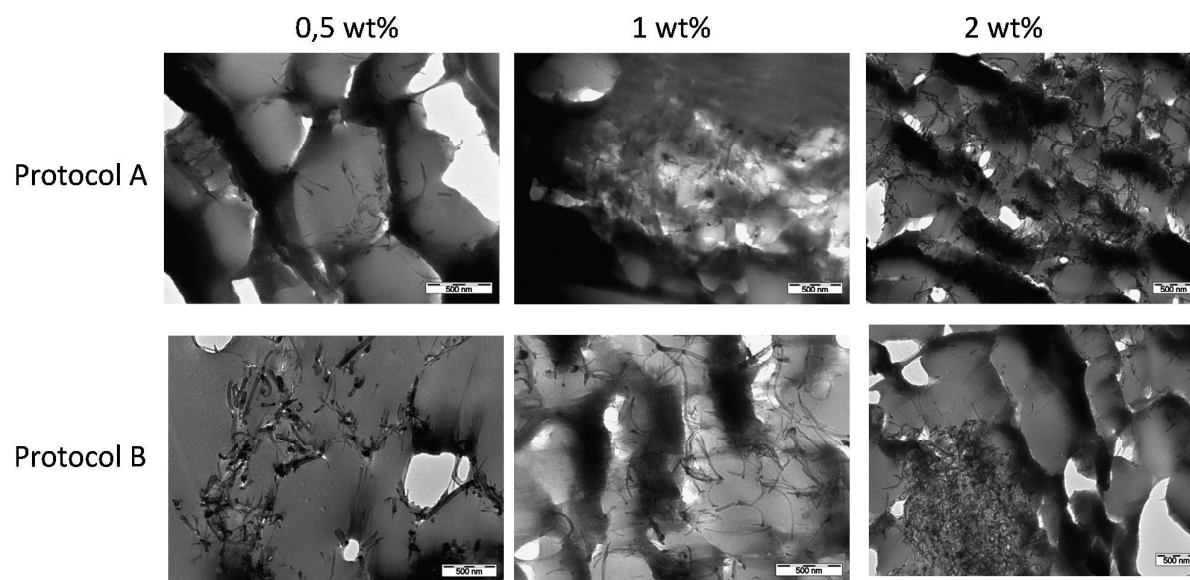


Figure 10

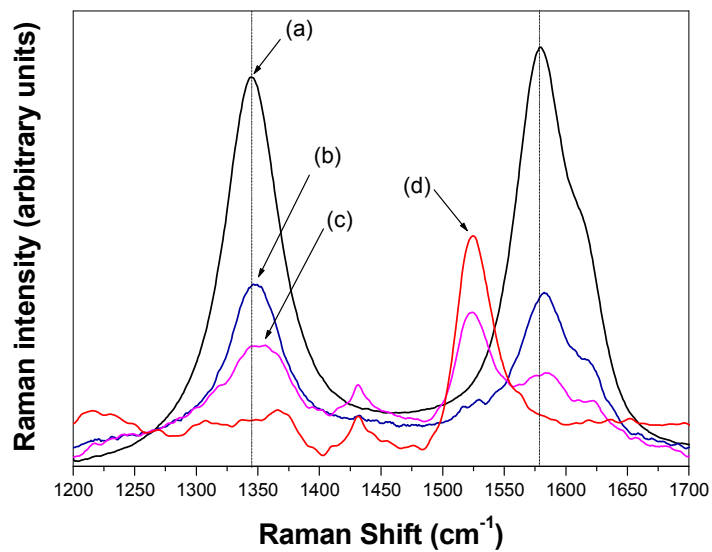


Figure 11

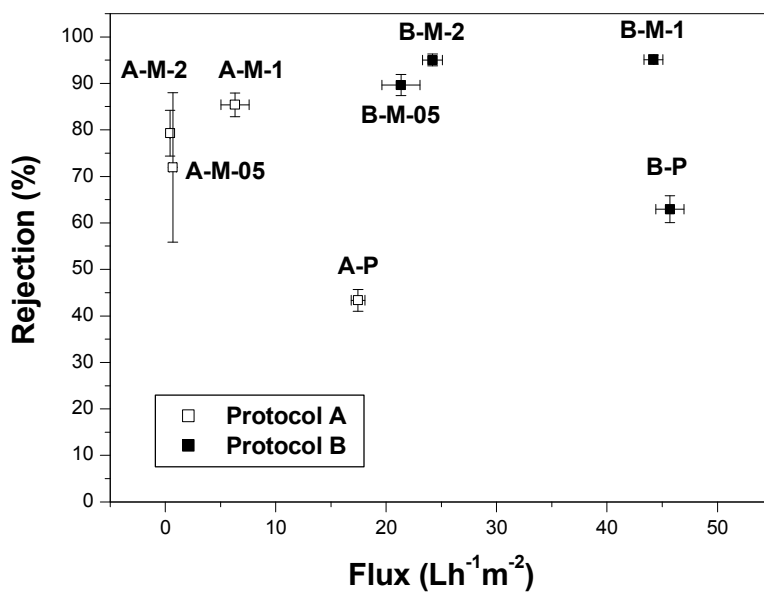
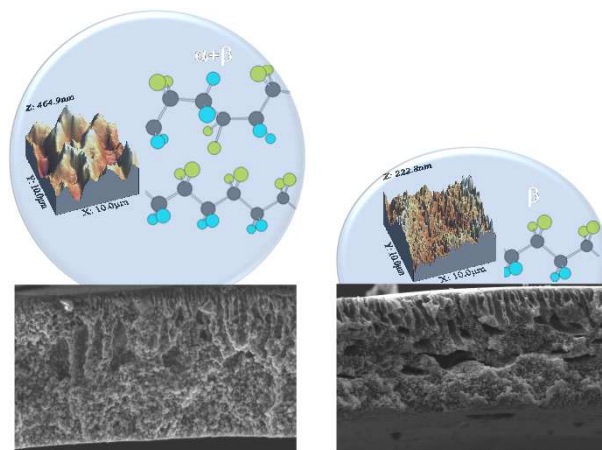


Figure 12



From hydrophobic to hydrophilic PVDF membranes by a combination of functionalization by blending chemical additives and selection of manufacturing procedure.